Biomass based porous carbon for supercapacitor by hydrothermal assisted activating method

Congcong Huang[1,*], Yunhui Dong[2] and Xingjun Dong[3]

[1]Department of Food Engineering, Shandong Business Institute, 264670 Yantai, P. R.China
[2]School of Chemistry and Chemical Engineering, Shandong University of Technology, 255049 Zibo, P. R. China
[3]Yantai Xinke Electronic Technology Co. LTD, 264000 Yantai, P. R.China

Abstract. A facile route has been employed to synthesize a series of high performance activated carbons as the electrode material for supercapacitors. The structure of the carbons are characterized by N_2 adsorption/desorption and FTIR spectroscopy. The electrochemical performances of the carbons as an electrode material were evaluated by cyclic voltammetry test and galvanostatic charge/discharge measurements. As a biomass derived carbon, KOH-1 exhibits high capacity, good rate capability and high energy density, indicating the promising application of hydrothermal combining with KOH activation method for biomass materials that used in supercapacitors.

1 Introduction

As the diminishing fossil fuels sources and emerging environmental issues, exploring alternative energy resources which are sustainable and renewable, like solar energy, wind power, tidal energy are urgently needed. Supercapacitors are of great interest due to the fact that they combine high power density with ultra-long cycle life and quick charge-discharge capability, properties that are currently lack in rechargeable batteries.

Undoubtedly, the successful commercial applications of supercapacitors are highly depended on suitable and superior electrode materials [1].Carbon materials are the most promising candidate owing to its high specific surface area, high conductivity and low cost. From the industry point of view, the large scale production of carbon materials in a sustainable way, renewable biomass based carbon is the primary feed stock.

Thus, recently a number of works have focused on using the by-products from food processing and agricultural industries as the precursors to prepare the carbon-based electrodes for supercapacitors. Various types of agricultural by-products like wheat straw [2], corncob [3], peanut shells [4] and rice husk [5] are in particularly interest because they are in the effort to reduce the production cost and preserve the environment.

Walnuts are the most productive nut in China with a yearly production of about 3.6 million tons [6]. Whereas the walnut shell are mainly used as fuels, which are the waste of resource. Consequently, there is a great need to convert walnut shells from waste to wealth. In this article, we used the walnut shell as the carbon precursor and a facile way was employed to develop a porous carbon with multiple organic functional groups which can be used in the supercapacitors.

2 Experimental

2.1 Chemicals

Walnut shell (<200μm), KOH, $ZnCl_2$, distilled water.

2.2 Preparation of carbon samples

The walnut shell (W) were sieved after mechanical crush to obtain particle sizes smaller than 200μm. Then the hydrothermal method was used to pretreatment the samples, in a typical preparation, a specific amount of solid activating agent (A) was dissolved in distilled water followed by add into 2 g of walnut shell powder and then the mixture was transferred into a Teflon threaded stainless steel autoclave, followed by heating the autoclave to 150°C for 12 h. Then the mixture was stirred at 100 °C to evaporate the water. When the mixture turned into muddy, transferred it into the tube furnace for activation at the temperature of 800 °C under N_2. Obtained products were washed with excess amount of 6M HCl under magnetic stirring and washed with distill water until the pH of the mixture was about 7.0 followed by filtration and drying. The prepared samples were denoted as A-X, where X represents the mass ratio of A/W. For example, KOH-3 means the mass ratio of the KOH:walnut shell is 3:1.

2.3 Physical characterization

The porous structure of the carbon samples were examined by N_2 sorption at 77 K using Micromeritics ASAP 2020 instrument. Specific surface areas were

* Corresponding author: huangcongcong@sdbi.edu.cn

calculated by using the BET (Brunauer-Emmett-Teller) equation. The total pore volume (V_T) was obtained at $P/P_0= 0.995$, and the pore size distribution was calculated by the BJH (Barrett, Joyner, Halender) method using the desorption branch of the isotherm. Before the measurements, all samples were degassed at 350°C under vacuum for 4h. FTIR spectroscopy (Nexus912A, Thermo Nicolet, USA) was used to investigate the functional groups on the carbon surface.

2.4 Electrode preparation and electrochemical evaluation

Samples were grounded with 5 wt% of PTFE (polytetrafluoroethylene) binder and pressed between two pieces of nickel foam under 300 kg/cm^2. Two electrodes were divided by insulating fiber-cloth (with thickness of 300 micrometers) and tested by cyclic voltammetry and galvanostatic charge-discharge measurements in CHI 660C electrochemical testing system. Both electrodes containing comparable masses, ca. 20 mg of carbon which were dried overnight at 100 °C under vacuum oven. The electrodes were impregnated with the electrolyte (30 wt% KOH) under vacuum to guarantee the thorough wetting.

3 Results and discussion

3.1 porous texture characterization

The adsorption and desorption isotherms of the samples were shown in Figure 1, it can be clearly seen that all the isotherms except for $ZnCl_2$-3 and $ZnCl_2$-4 exhibit the typically I isotherms, which means they can get a large absorbent amount below the pressure of 0.1 and reach a steady platform without hysteresis loops. It can be concluded that the pore of the carbon samples were mainly consist of abundant micropore and a small amount of mesopore. As for the isotherms of $ZnCl_2$-3 and $ZnCl_2$-4, they show type-IV curves with hysteresis loops at relative pressure above 0.4, which suggest the possession of abundant mesopore of the samples.

Pore-structure parameters of all studied carbons are listed in Table 1. It is found that the specific surface area reached a maximum value when the A/W is 3, further increasing the activation ratio, the S_{BET} decreased which may be caused by the collapse of the adjacent micropore. KOH-3 possesses the highest BET surface area, the micropore surface area and total pore volume, being 1862 m^2/g, 1496 m^2/g and 1.101 cm^3/g, respectively, which prove the effectiveness of KOH activation. We can assumed that the amount of mesopore and micropore can be controlled by adjusting the active agent ratio.
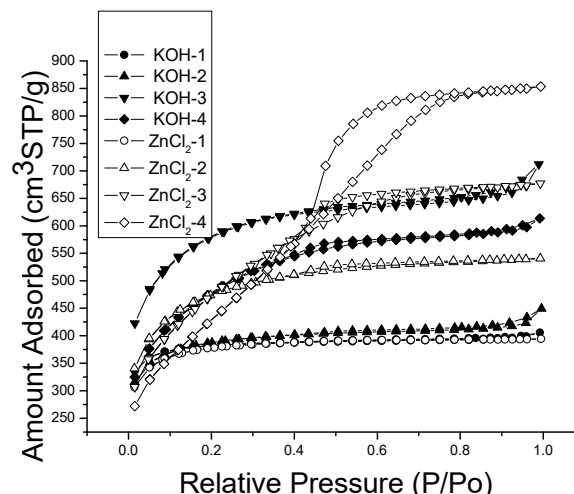

Figure 1. N$_2$ sorption isotherms of carbon samples.
Table 1. Surface area and pore-structure parameters of all samples.

Sample	A/W	S_{BET} (m^2/g)	S_{meso} (m^2/g)	S_{micro} (m^2/g)	V_T (cm^3/g)
KOH-1	1:1	1165	59	1106	0.628
KOH-2	2:1	1198	127	1071	0.695
KOH-3	3:1	1862	366	1496	1.101
KOH-4	4:1	1592	625	967	0.949
ZnCl$_2$-1	1:1	1163	82	1081	0.61
ZnCl$_2$-2	2:1	1498	332	1166	0.836
ZnCl$_2$-3	3:1	1641	1038	603	1.048
ZnCl$_2$-4	4:1	1549	1520	29	1.32

3.2 Electrochemical properties based on cyclic voltammetry measurements

Figure 2 show the CV profiles of all samples at the scan rate of 20mV/s and 100mV/s in 30% KOH electrolyte. At 20mV/s, all curves are standard rectangular shape which are typical for a stable double-layer capacitor within the voltage 0-0.9V[1]. At the scan rate of 100mV/s, the rectangular shape of all samples are maintained with only slight distortion, which shows the excellent capacitive behavior at high drain rate. The responded currents of the KOH activate carbons were larger than $ZnCl_2$ activate carbons, suggesting that KOH is more effective as an activation agent. Nevertheless, the surface area and the percentage of mesopore is relatively low compare to $ZnCl_2$ active samples, this phenomenon may be caused by the functional groups which generated by KOH activation.
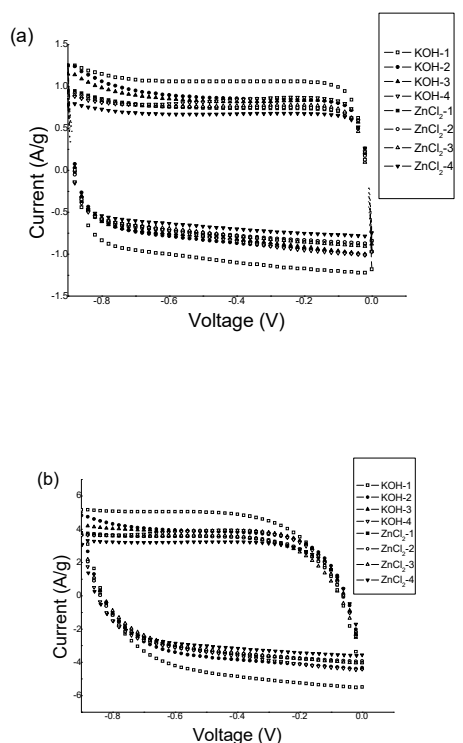
Figure 2. Cyclic voltammograms of all investigated samples recorded at the scan rates of 20 mV/s (a) and 100 mV/s (b)

3.3 Galvanostatic charge/discharge tests Colour illustrations

Galvanostatic charge–discharges with the current density of 20–200mA/cm^2 were conducted to obtain the specific capacitances of carbon samples. The corresponding specific capacitances were calculated by the equation :

$$C_{single} = \frac{I \times t}{\nabla V \times m} \qquad (1)$$

where I is the discharge current (mA), t is the total discharge time (s), m is the total mass of active material in both electrodes (g), V is the potential difference during the discharging (V) and Csingle is single-electrode specific capacitance (F/g).
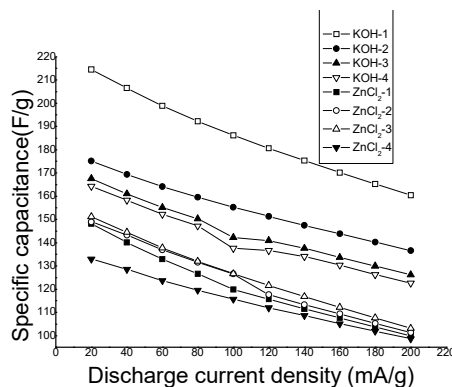
Figure 3. Comparison of capacitance decay with increasing discharge current density for all samples

As shown in Figure 3, KOH-1 shows the best performance and posses the largest specific capacitance of 215 F/g. At a low current density, the ions have enough time to diffuse into the micropore of the carbon, while at a higher current density the ions can only penetrate into part of micropores, which can explain why the capacitance of all the samples decrease as the current density increased gradually.
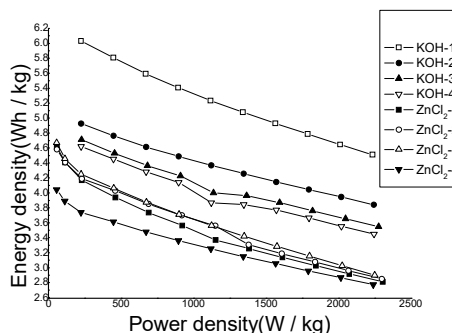
Figure 4. Ragone plots for all samples

The Ragone plots are frequently used in demonstration of power densities and energy densities of supercapacitors thus Figure 4 displays the plots for all investigated carbons. The energy density (in Wh/kg) is calculated as

$$E = \frac{1}{2}CV^2 \qquad (2)$$

where C is the capacitance of the two-electrode capacitor and V is the voltage decrease in discharge. The power (in W/kg) is calculated as

$$P = \frac{2E}{\Delta t_d} \qquad (3)$$

where E is the energy density and △td is the time spent in discharge.

In 30 wt% KOH aqueous electrolyte, the energy density of KOH series carbons are higher than $ZnCl_2$ series carbons at the same power density, which confirmed the effectiveness of KOH as an activation agent, However, at fast charge-discharge rates, only KOH-1 exhibits stable performance which means KOH-1 can release most of the energy under high discharge power conditions.

3.4 Surface functional characterization

It is obviously to see that KOH-1 and $ZnCl_2$-1 have the similar pore structure and pore size distribution according to Table 1, but the electric capacitive performance are quit different (as shown in the electrical measurement), this phenomena was speculate to be caused by the different surface chemistry or functional groups.
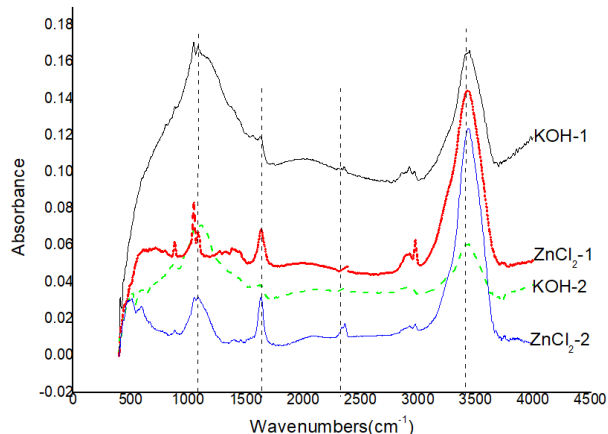
Figure5. FTIR spectra of KOH-1, KOH-2, $ZnCl_2$-1 and $ZnCl_2$-2

The FTIR spectra of KOH-1, KOH-2, $ZnCl_2$-1 and $ZnCl_2$-2 are shown in Figure 5. At the band of 1100 cm^{-1}, samples KOH-1 enhanced obviously compare to the other samples which was assigned to the C-O stretching vibration. It was found that for the $ZnCl_2$-1 and $ZnCl_2$-2, new bands appeared at 1625cm^{-1}, assigned to bending vibration of C=O, the broad band at 3450 cm^{-1} assigned to N-H stretching vibration, which enhanced obviously compare to the KOH activated samples. At the band of 2360 cm^{-1}, it was assigned to the CO_2. The results suggested that the surface functional groups varied in different samples. The surface functional groups on the carbon can affect the wettability, polarity and stability of carbon materials. The increase of wettability will be beneficial to the affinity of carbon surface to electrolyte ions, which will increase the ability of carbon surface to adsorb electrolytes, thus improving the ability of carbon material surface to form electric double layer, and thus improving the specific capacitance of the supercapacitors.

4 Conclusions

In this work, a series of carbons were synthesized by using hydrothermal assisted chemical activation of the walnut shell, KOH-1 shows the best electrochemical behavior with a specific capacitance of 215F/g in 30

wt% KOH electrolyte. It can be attributed to the enriched C-O functional groups and large mesopore structure of this carbon. Similarly, this method may shed some light on tailoring more biomass carbon materials for low cost and high-performance supercapacitors.

Acknowledgements

References

1. B.E.Conway, *Electrochemical Supercapacitors* (Kluwer-Plenum, New York, 1999)

2. G. Gou , F. Huang, M. Jiang, et al.[J]. Renew. Energy, **149**(2019)

3. Y. Shaoran, Z. Kaili , Nanomaterials, **8,** 4(2018):181

4. N. Yadav, M. K. Singh, N. Yadav, et al, J. Power Sources, **402** (2018):133-146

5. Z. Chen, X. Wang, B.Xue, etal., Carbon, **161**(2020): 432-444

6. http://www.csnc.cn/hangyedongtai/20200806104056. html